UV Resonance Raman Study of Angiotensin II Conformation in Nonaqueous Environments: Lipid Micelles and Acetonitrile

JANET S. W. HOLTZ, IGOR K. LEDNEV, SANFORD A. ASHER

Department of Chemistry, Chevron Science Center, University of Pittsburgh, Pittsburgh, Pennsylvania 15260

Received 25 November 1999; revised 22 June 1999; accepted 25 June 1999

ABSTRACT: We used 206.5-nm excited resonance Raman measurements to examine the angiotensin II (AII) secondary structure in H_2O in the presence of dodecylphosphocholine (DPC) micelles, sodium dodecylsulfate (SDS) monomers and micelles, and in a 70% acetonitrile (ACN-d)–30% water solution. Our AII-SDS titration absorption studies indicate the formation of a 1:2 AII:SDS complex in which two negatively charged SDS molecules attach to the AII positively charged N terminus and to Arg^2. Our 206.5-nm excited Raman results indicate that the 1:2 AII:SDS complexation increases the AII β-turn composition. We also used 228.9-nm Raman excitation to probe the local solvent accessibility of Tyr^4 (AII) in DPC and SDS micelles. Our Tyr (AII) solvent accessibility studies suggest that the Tyr residue is more exposed to the aqueous environment in SDS micelles than in DPC micelles. © 2000 John Wiley & Sons, Inc. Biopolymers (Biospectroscopy) 57: 55–63, 2000

Keywords: UV resonance Raman; angiotensin II; conformation; nonaqueous environments; lipid micelles; acetonitrile

INTRODUCTION

The octapeptide angiotensin II (AII), Asp-Arg-Val-Tyr-Ile-His-Pro-Phe, is the principal mediator of the renin-angiotensin system; AII induces an increase in blood volume and blood pressure via its actions at receptors in numerous target tissues.[1] When injected intravenously AII is the most potent natural elevator of blood pressure. This acute pressor effect is largely due to the ability of AII to cause arteriolar smooth muscle contraction. The renin-angiotensin system is believed to play an important role in regulating salt and water excretion by the kidney. Abnormalities in AII humoral pressor response can cause hypertension.[2]

A goal of the present study is to elucidate the conformations that AII could adopt as it docks at its receptor site. Knowledge of these conformations would be useful for designing new antihypertensive drugs.[3–5] This has motivated numerous previous AII secondary structural studies by various spectroscopic techniques (i.e., circular dichroism,[6,7] IR,[8,10] Raman,[8,10] fluorescence,[11] 2-dimensional NMR,[12] and X-ray diffraction[13]). Unfortunately, no study to date has characterized the receptor-bound AII conformation.

The biologically active conformation of AII at the receptor binding site is determined by the receptor site geometry and the local environment. It is believed that the environment around the AII receptor binding site at some point resembles a lipid–water interface, because the receptor binding site occurs at or near the epithelial

Correspondence to: S. A. Asher (asher+@pitt.edu).

Contract grant sponsor: NIH; contract grant number: R01GM30741.

Biopolymers (Biospectroscopy), Vol. 57, 55–63 (2000)

plasma membrane surface.[2,14] Therefore, the present examination of AII conformations in lipid environments that partially model the epithelial plasma membrane surface may yield likely receptor-bound AII conformations. Our laboratory previously examined the AII conformation in dodecylphosphocholine (DPC) lipid micelles, and we found an increased β-turn structure compared to that in water.[14,15]

In the work here we used 206.5-nm excited resonance Raman spectra to examine the environmental dependence of the AII secondary structure. DPC and sodium dodecyl sulfate (SDS) micelle studies probed the effect of different polar head groups on the AII secondary structure, and the aprotic solvent acetonitrile was used to mimic the hydrophobic environment within the interior of micelles. We also used absorption studies to determine the AII : SDS complexation ratio and to relate this fatty acid complexation to the observed increased AII β-turn structure. In addition, we utilized a new methodology, which determines Tyr water accessibility from 228.9-nm Tyr Raman cross section measurements, to determine the solvent accessibility of the Tyr ring of AII in H_2O, DPC, and SDS micelles.[16]

EXPERIMENTAL

Materials

The AII and *N*-acetyl-tyrosine-ethyl ester (Ac-Tyr-EE) were purchased from Sigma Chemical Co. The DPC was obtained from Avanti Polar Lipids, Inc. The SDS was purchased from Mallinckrodt. Acetonitrile-d_3 (ACN-d) and sodium perchlorate were purchased from Aldrich. The D_2O was purchased from Cambridge Isotope Laboratories. These compounds were used as received.

Sample Preparation

206.5-nm Raman Excitation

The AII (0.66 m*M*) dissolved in H_2O containing 0.20*M* $NaClO_4$ was added to DPC and SDS surfactant solutions to yield 148 m*M* DPC and 173 m*M* SDS solutions. Aliquots of 1.49 m*M* aqueous AII containing 0.67*M* $NaClO_4$ was added to 30 and 70% ACN-d–H_2O mixtures to yield final 0.45 m*M* AII and 0.20*M* $NaClO_4$ concentrations.

228.9-nm Raman Excitation

Aqueous solutions of AII ($\sim$1.3 m*M*) in the presence of 0.22*M* $NaClO_4$ were added to solid DPC and solid SDS. Above the critical micelle concentration (cmc) of 1 and 8.2 m*M*, DPC and SDS form micelles with aggregation numbers of 40 and 64, respectively.[17,18] Aliquots of 2.4 m*M* aqueous AII containing 0.67*M* $NaClO_4$ were added to ACN-d–H_2O mixtures to give final concentrations of $\sim$0.8 m*M* AII and 0.20*M* $NaClO_4$ in the 10, 20, 30, 50, and 70% ACN-d–H_2O mixtures.

Instrumentation

UV-Visible (UV-Vis) Absorption

Absorption spectra were measured in 0.5-mm pathlength cells by using a Perkin–Elmer Lamda 9 UV-Vis-NIR spectrophotometer.

UV Resonance Raman Spectroscopy

We utilized $\sim$2.2 mW of 228.9-nm excitation from an intracavity frequency doubled CW argon ion laser to examine the solvent accessibility of the AII Tyr residue.[19] We used $\sim$1.1 mW of 206.5-nm excitation from an intracavity frequency doubled CW krypton ion laser to excite within the amide π–π^* transitions in order to selectively enhance the amide vibrations.[15] The Raman scattered light was collected in a 135° backscattering geometry from a spinning quartz cell containing $\sim$0.5 mL of peptide solution, and it was dispersed by a Spex TripleMate spectrograph with an 1800 groves/mm spectrograph grating.[20,21] The spectra were detected with an intensified CCD detector (Princeton Instruments, Inc., model ICCD-1024 MS-E). The total accumulation time for the 228.9- and 206.5-nm excited Raman spectra were 3 and 9 min, respectively. The spectral resolution of the 228.9- and 206.5-nm Raman spectra were $\sim$9 and $\sim$11 cm^{-1}, respectively.

RESULTS AND DISCUSSION

UV-Vis Absorption of AII

Figure 1(A) shows the UV-vis spectrum of a 1.3 m*M* AII solution in H_2O. The broad features centered around 275 nm derive from the Tyr $L_b \leftarrow A_{1g}$ π–π^* transition with a small contribution from the Phe $L_b \leftarrow A_{1g}$ π–π^* electronic transition at $\sim$257 nm.[4,22,23] The increase in absorption below 240 nm derives mainly from Tyr and Phe

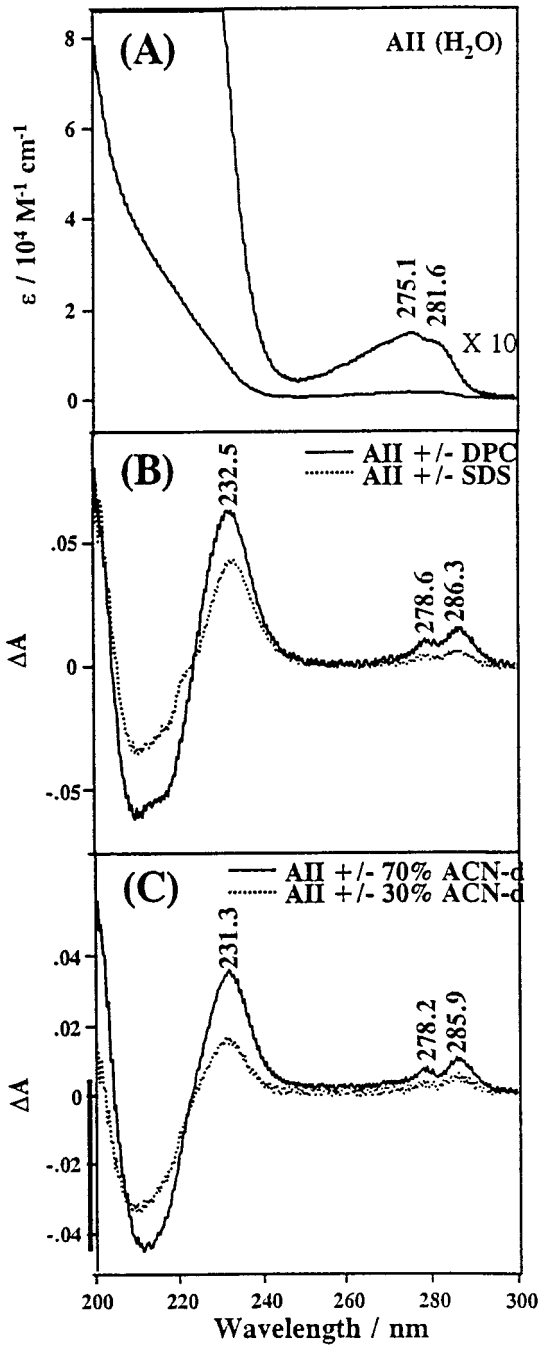

Figure 1. (A) The absorption spectrum of 0.66 m*M* AII in H_2O at pH 6.9; (B) 0.66 m*M* AII absorption difference spectra induced by 148 m*M* DPC (1 AII/5.5 DPC micelles) and 173 m*M* SDS (1 AII/4 SDS micelles); (C) 0.45 m*M* AII absorption difference spectra induced by 70 and 30% ACN-d–H_2O mixtures. The absorption spectra are measured in 0.5-mm cells.

electronic transitions. However, the absorption below 220 nm also includes contributions from His, Pro, and peptide amide π–π^* transitions.[24–26]

Figure 1(B) shows the absorption difference spectra of AII in DPC and SDS micelles relative to that of AII in pure H_2O. Absorption difference bands at ~232.3, 278.6, and 286.3 nm are due to Tyr absorption red shifts. The absorption difference spectra for AII in DPC and SDS micelles are similar to those observed by Cho and Asher of AII in DPC micelles.[14] A similar Tyr absorption red shift is also observed with increasing ACN-d concentration [Fig. 1(C)].

We titrated a 0.54 m*M* AII solution with increasing SDS concentrations ranging from 0.27 to 227 m*M* (cmc of SDS = 8.2 m*M*). Figure 2 shows the absorption difference spectra of 0.54 m*M* AII as a function of increasing SDS concentrations. A significant Tyr absorption red shift occurs at ~2 m*M* SDS, and further Tyr absorption differences increase with increasing SDS concentrations. Our modeling study indicates the formation of a 1:2 AII:SDS complex for SDS concentrations below the cmc (see Appendix). In addition, we found that above the SDS cmc there is an additional partitioning of the AII:SDS complex into individual SDS micelles with an association constant of $1800M^{-1}$ (see Appendix).

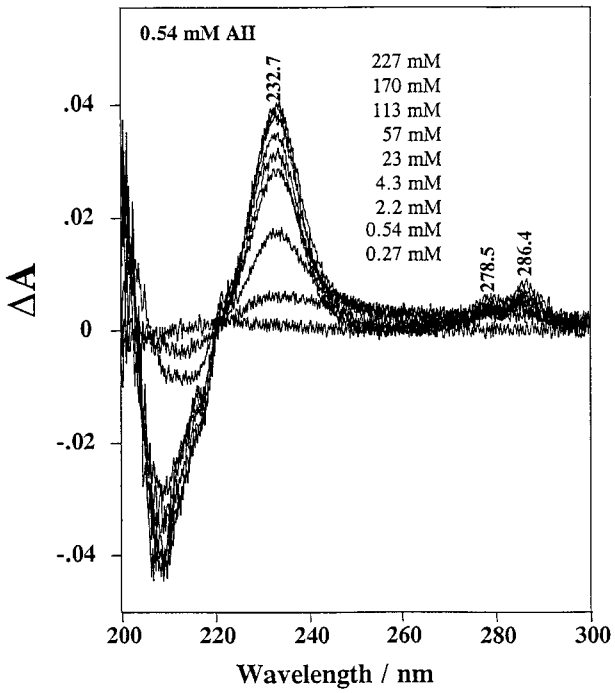

Figure 2. The absorption difference spectra of 0.54 m*M* AII in H_2O as a function of increasing SDS concentrations. The SDS concentrations are 0.27, 0.54, 4.3, 23, 57, 113, 170, and 227 m*M* SDS. Absorption spectra are measured in 0.5-mm cells.

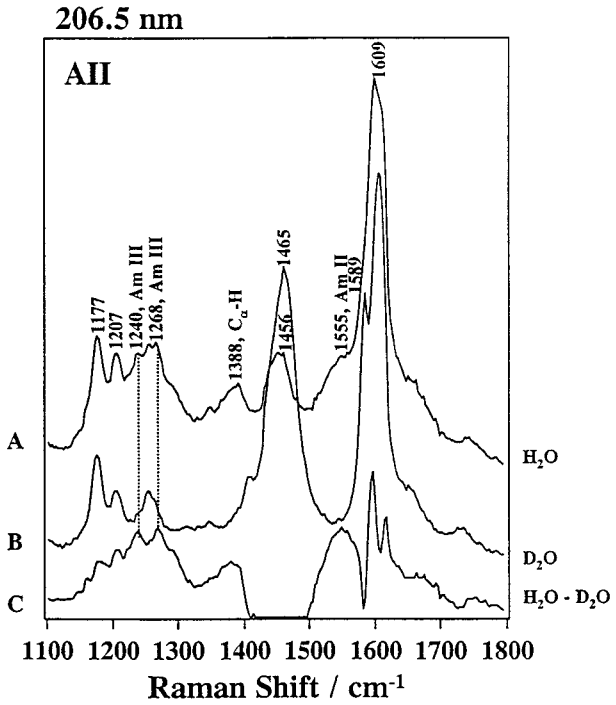

Figure 3. The 206.5-nm excited Raman spectra of 0.66 m*M* AII dissolved in (A) pure H_2O or (B) D_2O and (C) their Raman difference spectrum; ~ 1.1 mW of 206.5-nm light was focused onto the sample. The spectra were detected by an ICCD detector with a total accumulation time of 9 min and a spectral resolution of ~ 11 cm^{-1}.

AII Secondary Structure

Figure 3 shows the 206.5-nm excited Raman spectra of AII in H_2O and D_2O and the difference spectrum between AII in H_2O and D_2O. The 206.5-nm excitation occurs directly in the backbone amide π–π^* transitions, which results in enhancement of amide vibrations.[26] There are, however, some spectral contributions from Phe and Tyr residues in the 1200–1300 and 1580–1620 cm^{-1} regions, which overlap with the amide III and amide I spectral regions, respectively. In D_2O the deuterium exchange of the amide N—H bond dramatically changes the amide normal mode composition. This exchange allows us to unequivocally assign the amide I, II, and III bands of the protonated species despite the overlap with Phe and Tyr contributions [Fig. 3(C)].

In Figure 3(A) the most intense band (1609 cm^{-1}) derives from overlapping Phe and Tyr ν_8 vibrational bands.[27,28] The bands at 1177 and 1207 cm^{-1} are mainly due to the Tyr ν_{9a} and ν_{7a} vibrations with some contribution from Phe. There is also some contribution from the Tyr $\nu_{7a'}$ band at 1266 cm^{-1}. Upon deuteration the 1609 cm^{-1} band splits into bands at 1589 and 1609 cm^{-1}. The 15,890 cm^{-1} band is ascribed to the overlap of Phe ν_{8b} and the downshifted Tyr ν_{8b}.[28] In addition, in the presence of D_2O the Tyr $\nu_{7a'}$ band downshifts to 1258 cm^{-1}.

The amide III (1240–1280 cm^{-1}) region consists of a broad band with spectral features at 1240 and 1268 cm^{-1}. The amide III vibrational normal mode derives from a combination of C—N stretching and N—H bending motions. However, deuteration of the amide proton decouples the C—N stretching from N—H bending, and the amide III band disappears. In Figure 3(A) most of the 1268 cm^{-1} band intensity can be confidently assigned to the amide III vibration, because upon deuteration the 1268 cm^{-1} band mostly disappears from the spectrum [Fig. 3(B)]. The difference spectrum [Fig. 3(C)] indicates that the 1240 cm^{-1} band also derives from an amide III vibration.

The shoulder at ~1555 cm^{-1} is assigned to the amide II vibration, which also disappears in D_2O (Fig. 3), because it also contains C—N stretching and N—H bending. The intense amide II′ band (1465 cm^{-1}) overlaps the CH_2 deformation vibration band at 1456 cm^{-1}.

The amide III band at 1240 cm^{-1} in Figure 3 suggests the existence of a β sheet in pure water.[14] Furthermore, the amide III band at 1268 cm^{-1} suggests the presence of random coil and some β-turn structures.[14] Little α-helical structure is present in aqueous AII as is indicated by the intensity of the 1388 C_α—H bend band.[26,27,29] Cho and Asher previously showed that AII exists in multiple conformations in pure H_2O.[14]

Nonpolar solvents are often used as a model system to examine peptide interactions with biological membranes.[30] Previous studies demonstrated secondary structural differences between AII in a hydrophobic medium compared to that in water.[14,30,31] In this study we compared the AII structure in the presence of negatively charged and zwitterionic lipids. Figure 4 shows the 206.5-nm excited Raman spectra of AII in a 173 m*M* SDS solution (far above the 8.2 m*M* cmc) and in pure H_2O and their difference spectrum. Partitioning of AII into SDS micelles (vide infra) alters the amide III spectral region as observed in the difference spectrum [Fig. 4(C)]. The appearance of the 1274 cm^{-1} amide III band can be assigned to an increased β-turn structure.[14,28]

Figure 5 demonstrates an increased AII β-turn

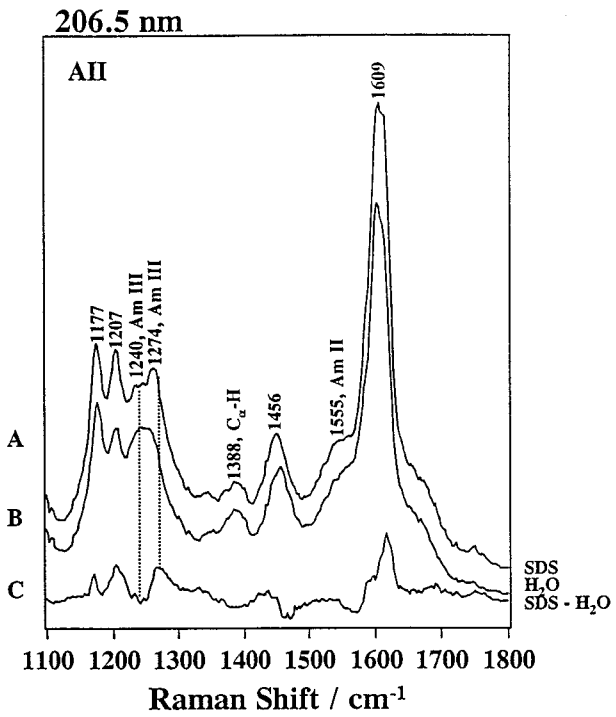

Figure 4. The 206.5-nm excited Raman spectra of 0.66 m*M* AII dissolved in (A) 173 m*M* SDS or (B) pure H_2O and (C) their Raman difference spectrum. Laser power, total accumulation time, and the spectral resolution are the same as Figure 2.

structure 1274 cm^{-1} band intensity in the presence of DPC micelles, SDS micelles, and monomeric SDS, as well as in a 70% ACN-d–30%H_2O mixture. A similar DPC micelle difference spectrum was observed by Cho and Asher.[14] We compared the 1274 cm^{-1} band intensities for AII in SDS and DPC micelles and found an ~15% decreased fractional abundance of β-turn structure in SDS micelles compared to that in DPC micelles. This difference is not the result of lower partitioning of AII into SDS micelles, because the SDS association constant is larger (see Appendix). Because the DPC and SDS micelles have essentially identical hydrophobic interiors, it is likely that the polar head group difference alters the binding of AII in the micelle, which in turn alters the fractional abundance of the β-turn structure.

Our absorption measurements demonstrate tight binding of two SDS monomers to each AII molecule. Figure 5 demonstrates the increase in the 1274 cm^{-1} band intensity upon binding to two SDS molecules, while Figure 6 shows the SDS dependence of the fractional AII β-turn structure relative to the maximum AII β-turn structure that occurs in DPC micelles. At 173 m*M* SDS the AII β-turn content is ~85% of the maximum β-turn observed for AII in DPC micelles, while at 8 m*M* SDS, just below the cmc, the AII β-turn content is ~60% of the maximum observed in DPC micelles. Thus, our AII-SDS absorption and Raman studies indicate that ~66% of the AII β-turn formation results from AII complexation to two SDS monomers, while an additional 33% β-turn formation results from AII partitioning into the SDS micelle interior (Fig. 6).

Hydrophobic environments were previously shown to induce AII conformational changes.[30] We examined the AII secondary structure dependence on environmental hydrophobicity by examining AII in ACN-d–H_2O mixtures [Fig. 5(F)]. We found that, although a 70% ACN-d–30% H_2O mixture induces a β-turn structure, the β-turn fractional abundance is ~25% less than that induced by DPC micelles. We were unable to examine

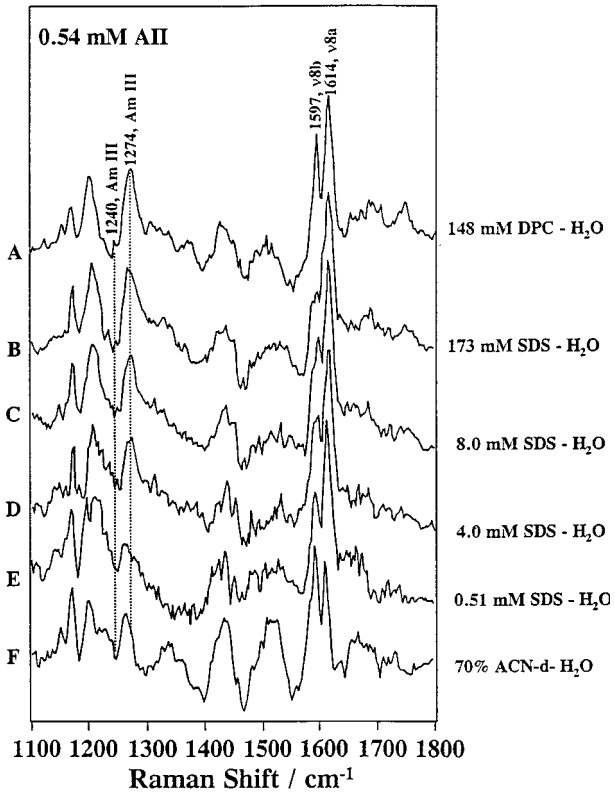

Figure 5. The 206.5-nm excited Raman difference spectra of 0.54 m*M* AII in pure H_2O and in the presence of (A) 148 m*M* DPC, (B) 173 m*M* SDS, (C) 8.0 m*M* SDS, (D) 4.0 m*M* SDS, (E) 0.51 m*M* SDS, and (F) 70% ACN-d–30% H_2O mixture. The 1274 cm^{-1} band intensity correlates with an increased AII β-turn structure.

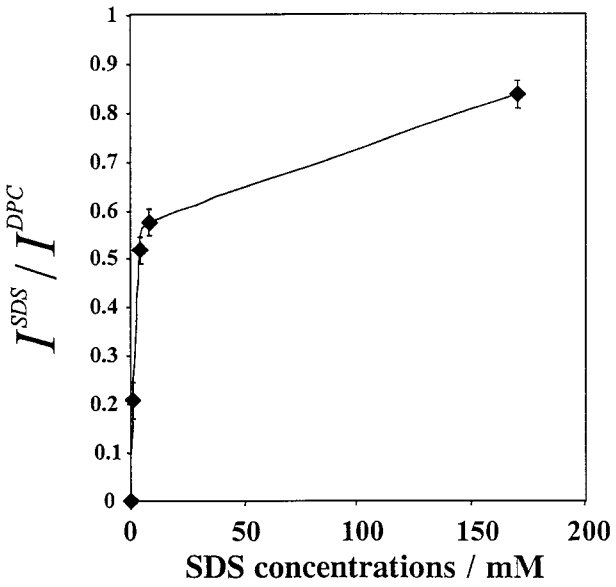

Figure 6. The plot of the 1274 cm^{-1} band intensity of AII in SDS ratioed to the 1274 cm^{-1} band intensity of AII in 143 m*M* DPC as a function of SDS concentrations.

higher ACN-d concentrations due to insufficient AII solubility.

AII Tyr Water Exposure

Figure 7 shows the 228.9-nm excited Raman spectra of AII in H_2O, SDS, and DPC micelles. The 932 cm^{-1} band derives from ClO_4^-, the internal standard. The Tyr Raman bands dominate because of resonance with the 222-nm ($L_a \leftarrow A_{1g}$) Tyr absorption band.[22,23] The contribution of Phe is less than 5% for 228.9-nm excitation.[14,32] The Raman bands at 1174, 1203, and 1614 cm^{-1} derive from the Tyr ν_{9a}, ν_{7a}, and ν_{8a} vibrations, respectively.

The Tyr 1614 cm^{-1} band shows an ~13% intensity increase in the presence of 152 m*M* DPC and an ~12% band intensity increase in the presence of 172 m*M* SDS compared to pure H_2O (Fig. 7). The 1614 cm^{-1} Tyr band intensity increases by ~12% in the 70% ACN-d aqueous solution relative to that in pure H_2O (spectrum not shown). These increased Tyr Raman band intensities result from red shifts of the AII Tyr absorption bands in the DPC and SDS micelles and in the ACN-d–H_2O mixtures [Fig. 1(B,C)].

Chi and Asher discovered a direct correlation between the Raman cross section of the Tyr 1614 cm^{-1} (ν_{8a}) band, σ_{cal} ($\Delta\nu$, ν_{ex}), and the water accessibility of the phenolic ring.[16] This correlation results from the dependence of the Tyr absorption λ_{max} values to H_2O exposure. Equation (1) allows us to correlate the Tyr absorption band shifts relative to water to changes in the Raman cross sections. In turn, we can correlate these absorption band shifts to changes in the Tyr water exposure. Equation (1) relates the Raman cross sections σ_{cal} ($\Delta\nu$, ν_{ex}) (cm^2/mol · str):

$$\sigma_{cal}(\Delta\nu,\ \nu_{ex}) = \frac{32380}{(43786 - \Delta\nu - \nu_{ex})^2 + 221800} + \frac{594500}{(44758 - \Delta\nu - \nu_{ex})^2 + 675700} + \frac{7250}{(46123 - \Delta\nu - \nu_{ex})^2 + 28900} \quad (1)$$

where ν_{ex} (cm^{-1}) is the Raman excitation frequency and $\Delta\nu$ (cm^{-1}) is the absorption band solvent shift for Tyr compared to that in water. See Chi and Asher for further details.[16]

Our results show that the Raman cross section

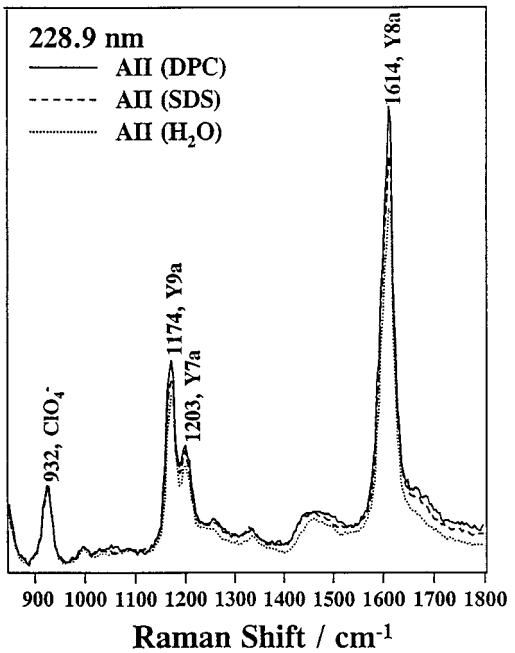

Figure 7. The 228.9-nm excited Raman spectra of ~1.3 m*M* AII dissolved in (· · ·) pure H_2O, (- - -) 172 m*M* SDS, and (—) 152 m*M* DPC micelles. The 932 cm^{-1} band derives from the 0.22*M* sodium percholate internal standard; ~ 2.2 mW of 228.9-nm light was focused onto the sample. The spectra were detected by an ICCD detector with a total accumulation time of 3 min and a spectral resolution of ~ 9 cm^{-1}.

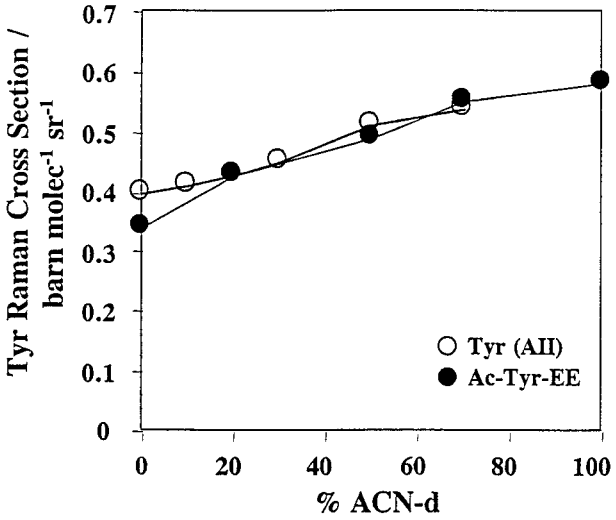

Figure 8. The dependence of 228.9-nm excited Raman cross sections of the (○) AII Tyr 1614 cm^{-1} band and (●) Ac-Tyr-EE on ACN-d concentration.

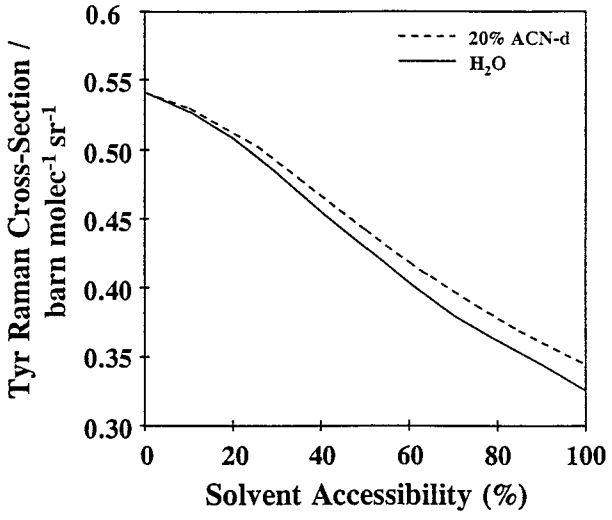

Figure 9. The calculated dependence of the 228.9-nm excited Tyr Raman cross sections to their solvent accessibility. (—) The curve was calculated assuming the Tyr residue is surrounded by either pure H_2O or valine residues. (- - -) For the 20% ACN-d–80% H_2O mixture we assume that for 100% solvent accessibility the Tyr would be fully exposed to a 20% ACN-d–80% H_2O mixture. See Chi and Asher for details.[16]

of Tyr in AII increases with increasing ACN-d concentration (Fig. 8, Table I). These increased Raman cross sections result from red shifts of the Tyr absorption with increasing ACN-d concentrations. We also observed similar increases in the Ac-Tyr-EE Raman cross sections with increasing ACN-d concentrations (Fig. 8).

Utilizing Chi and Asher's approach,[16] we can estimate the magnitude of the Tyr (AII) solvent exposure in a particular ACN–H_2O solution by comparing the observed Raman cross section to the calculated dependence of the Raman cross section on the Tyr ring exposure to this solvent. Chi and Asher[16] calculated the dependence of the Tyr Raman cross sections to water exposure for a Tyr residue that is surrounded by either water or valine side chains (solid line in Fig. 9). We similarly calculated the Raman cross section dependence for Tyr either exposed to valine side chains or to a 20% ACN-d–80% H_2O solution (dashed line in Fig. 9). The measured 0.43 barn/mol sr Tyr (AII) Raman cross section in 20% ACN-d solution indicates a Tyr solvent accessibility of ~60%, and for AII dissolved in pure H_2O the measured 0.40 barn/mol sr Tyr (AII) Raman cross section indicates a 62% water accessibility. These results suggest that the Tyr ring is partially buried in the AII peptide. These estimated accessibilities probably have a relative accuracy of 10%.

In the presence of 148 m*M* DPC and 173 m*M* SDS (far above their cmc's) the 0.54 and 0.52 barn/mol sr Raman cross sections of the Tyr (AII) 1614 cm^{-1} band are much larger than the 0.40 barn/mol sr expected in pure H_2O (Table II). These increased Tyr (AII) Raman cross sections indicate burial of the Tyr by the DPC and SDS micelles. We used Figure 9 (solid line) to estimate that the Tyr is 0 and 15% exposed to water in the DPC and SDS micelles, respectively. Because the Tyr absorption difference for the 1:2 AII:SDS complex is roughly half of that in the SDS micelles (170 m*M* SDS) (Fig. 2), we can roughly estimate an AII Tyr water accessibility for the 1:2 AII:SDS complex to be ~40%.

The slightly higher Tyr (AII) water accessibility in SDS micelles compared to DPC micelles

Table I. Calculated (*c*) and Measured (*m*) Tyr (AII) Raman Cross Sections in Various ACN-d Concentrations

ACN-d (%)	0	10	20	30	50	70
$\sigma_{Tyr,c}$ (barn/mol sr)	0.46	0.50	0.53	0.55	0.60	0.66
$\sigma_{Tyr,m}$ (barn/mol sr)	0.40	0.41	0.43	0.45	0.51	0.54

Table II. Measured Tyr (AII) Raman Cross Section and Solvent Accessibility of AII in H_2O, DPC, and SDS Micelles

	H_2O	DPC	SDS
σ_{Tyr} (barn/mol sr)	0.40	0.54	0.52
Solvent accessibility (%)	62	0	15

may derive from charge interactions between the positively charged AII sites and the negatively charged SDS polar head group. This interaction would constrain SDS-bound AII closer to the water–micelle interface compared to DPC-bound AII. This should cause the Tyr residue to localize closer to the water–micelle interface.

The complexation of AII to the anionic SDS monomers demonstrates the ability of negatively charged lipids to alter the AII structure. We postulate that the attachment of the negatively charged SDS molecules to the positively charged NH_3^+ terminus and the Arg^2 residue also results in the association of the SDS alkyl chains with the nonpolar Val^3, Tyr^4, Ile^5, Pro^7, and Phe^8 residues to form a hydrophobic domain. This is likely to be the driving force for the formation of the β turn; formation of this turn permits the formation of a more compact hydrophobic domain.

It is possible that similar AII charge interactions with anionic receptor groups play a role in binding to the receptor site. This possibility is supported by Moore's demonstration that replacement of Arg^2 by Gly^2 greatly diminishes the AII receptor binding affinity.[1]

CONCLUSION

Our results suggest that hydrophobic interactions between AII and lipids and apolar environments result in an increased β-turn composition. Our AII-SDS absorption and Raman studies indicate that the charge-induced binding between two positively charged AII side chains and two negatively charged SDS monomers result in a complex that has approximately two-thirds of the increased AII β-turn conformation observed in SDS micelles, while the remaining increase in the β turn results from partitioning into the SDS micelle interior.

The 228.9-nm Raman solvent accessibility studies of the AII Tyr in DPC and SDS micelles suggest that the Tyr residue lies closer to the water–micelle interface in SDS micelles compared to DPC micelles because of the binding of AII's positively charged amino terminus and Arg^2 to the negatively charged SDS head groups.

We would like to thank Dr. Zhenhuan Chi for helpful discussions.

APPENDIX

Our AII-SDS titration absorption studies show that significant SDS-induced Tyr absorption red shifts occur at concentrations far below the SDS cmc (SDS_{cmc} = 8.2 mM). This indicates formation of AII-SDS complexes (Fig. A.1). We model the SDS binding as

$$\mathrm{AII} + nS_{\mathrm{SDS}} \underset{K}{\leftrightarrow} \mathrm{AII} \cdot \mathrm{SDS}_n, \qquad \text{(A.1)}$$

where n is the number of SDS molecules complexed to each AII molecule. The AII-SDS complexation ratio and the binding constant, K can be determined by modeling the AII-SDS binding curve:

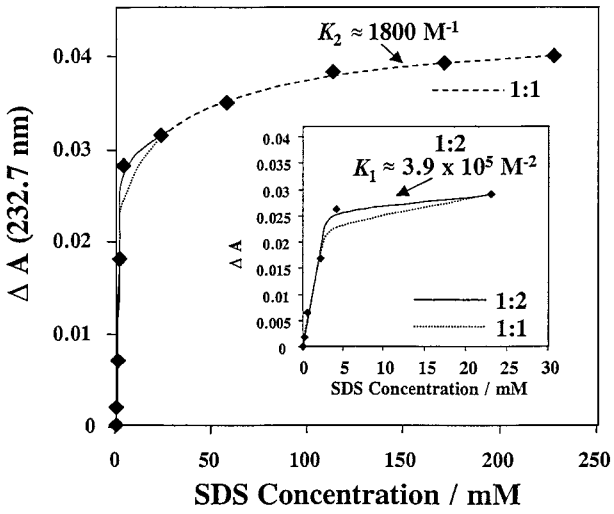

Figure A.1. The SDS concentration dependence of the 232.7-nm Tyr absorption intensity difference between AII in the presence and absence of SDS. The inset shows an expanded scale for SDS concentrations below the cmc. The dotted line is the theoretical best fit of Eq (3) for $n = 1$. (—) The best fit for $n = 2$ and a binding constant $K_1 = 3.9 \times 10^5\ M^{-2}$ (- - -) For SDS concentration above 8.2 mM, the AII-micelle SDS association curve can be modeled using Eq (3) for $n = 1$ and with an association constant of $K_2 = 1800\ M^{-1}$, where the lipid micelle concentration is determined by the ratio of the lipid concentration to the micelle aggregation number of 64.[18]

$$K = \frac{M_b}{(1 - M_b)(S_0 - nM_bP_0)^n}, \qquad (A.2)$$

where M_b is the mole fraction of AII bound to SDS molecules, S_0 is the initial SDS concentration, P_0 is the initial peptide concentration, and n is the binding stoichiometry.

The calculated AII-SDS binding curve (dotted line) for $n = 1$ gives a poor fit to the experimental results (Fig. A.1 inset graph), while $n = 2$ (solid line) gives a very good fit. [Note: the calculated AII-SDS binding curve (solid line) is for SDS concentrations up to 23 mM SDS.] This modeling indicates an AII:SDS complexation ratio of 1:2 with a binding constant of $K_1 = 3.9 \times 10^5\ M^{-2}$. It is likely that the negatively charged head groups of the two SDS molecules attach to the positively charged AII N terminus and to the Arg^2 residue. We did not see a similar complexation of zwitterionic DPC monomers to AII.

We also used Eq. (3) to model the AII-SDS association curve for SDS concentrations above the cmc, where we utilized the lipid micelle concentration given by the ratio of the lipid concentration to the micelle aggregation number (64 SDS/micelle).[18] We obtained a good fit using $n = 1$, which suggests that one AII partitions into each SDS micelle with an association constant of $K_2 = 1800\ M^{-1}$. Cho and Asher previously determined an AII-DPC micelle association constant of 610 M^{-1}.[14]

REFERENCES

1. Moore, G. J. Comprehen Med Chem 1990, 3, 961–980.
2. Peach, M. J. In Angiotensin and Blood Pressure Regulation; Harding, J. W., Wright, J. W., Spety, R. C., Barnes, C. D., Eds.; Academic Press: New York, 1988; p 35–60.
3. Hondrelis, J.; Matsoukas, J.; Agelis, G.; Cordopatis, P.; Zhou, N.; Vogel, H.; Moore, G. J. Collect Czech Chem Commun 1994, 59, 2523–2532.
4. Joseph, M. P.; Maigret, B.; Scheraga, H. A. Int J Peptide Protein Res 1995, 46, 514–526.
5. Shin, Y. A.; Yoo, S.-E. Biopolymers 1996, 38, 183–190.
6. Lintner, K.; Fermandjian, S.; Fromageot, P.; Khosla, M. C.; Smeby, R. R.; Bumpus, F. M. Biochemistry 1977, 16, 806–812.
7. Piriou, F.; Lintner, K.; Fermandjian, S.; Fromageot, P.; Khosla, M. C.; Smeby, R. R.; Bumpus, F. M. Proc Natl Acad Sci USA 1980, 77, 82–86.
8. Fermandjian, S.; Fromageot, P.; Tistchenko, A. M.; Leichnam, J. P.; Lutz, M. Eur J Biochem 1972, 28, 174–182.
9. Surewicz, W. K.; Mantsch, H. H. J Am Chem Soc 1988, 110, 4412–4414.
10. Fox, J. W.; Tu, A. T. Arch Biochem Biophys 1980, 201, 375–383.
11. Turner, R. J.; Matsoukas, J. M.; Moore, G. J. Biochim Biophys Acta 1991, 1065, 21–28.
12. Cushman, J. A.; Mishra, P. K.; Bothner-By, A. A.; Khosla, M. S. Biopolymers 1992, 32, 1163–1171.
13. Garcia, K. C.; Ronco, P. N.; Verroust, P. J.; Brunger, A. T.; Amzel, L. M. Science 1992, 257, 502–507.
14. Cho, N.; Asher, S. A. Biospectroscopy 1996, 2, 71–82.
15. Holtz, J. S. W.; Bormett, R. W.; Chi, Z.; Cho, N.; Chen, X. G.; Pajcini, V.; Asher, S. A.; Spinelli, L.; Owens, P.; Arrigoni, M. Appl Spectrosc 1996, 50, 1459–1468.
16. Chi, Z.; Asher, S. A. J Phys Chem B 1998, 102, 9595–9602.
17. Inagaki, F.; Shimada, I.; Kawaguchi, K.; Hirano, M.; Terasawa, I.; Ikura, T.; Go, N. Biochemistry 1993, 28, 5985–5991.
18. Rosen, M. J. In Surfactants and Interfacial Phenomena, 2nd ed.; Wiley: New York, 1989; p 116.
19. Asher, S. A.; Bormett, R. W.; Chen, X. G.; Lemmon, D. H.; Cho, N.; Peterson, P.; Arrigoni, M.; Spinelli, L.; Cannon, J. Appl Spectrosc 1993, 47, 628–633.
20. Asher, S. A.; Johnson, C. R.; Murtaugh, J. Rev Sci Instrum 1983, 54, 1657–1662.
21. (a) Asher, S. A. Anal Chem 1993, 65, 59A–66A; (b) Asher, S. A. Anal Chem 1993, 65, 201A–210A.
22. Asher, S. A.; Ludwig, M.; Johnson, C. R. J Am Chem Soc 1986, 108, 3186–3197.
23. Fodor, S. P. A.; Copeland, R. A.; Grygon, C. A.; Spiro, T. G. J Am Chem Soc 1989, 111, 5509–5518.
24. Dudik, J. M.; Johnson, C. R.; Asher, S. A. J Phys Chem 89, 1985, 3805–3814.
25. Copeland, R. A.; Spiro, T. G. Biochemistry 1987, 26, 2134–2139.
26. Song, S.; Asher, S. A. J Am Chem Soc 1989, 111, 4295–4305.
27. Hildebrandt, P. G.; Copeland, R. A.; Spiro, T. G. Biochemistry 1988, 27, 5426–5433.
28. Takeuchi, H.; Ohtsuka, Y.; Harada, I. J Am Chem Soc 1992, 114, 5321–5328.
29. (a) Tu, A. T. In Spectroscopy of Biological Systems; Clark, R. J. H.,; Hester, R. E., Eds.; Wiley: Chichester, UK, 1986; p 47–112; (b) Harada, I.; Takeuchi, H. In Spectroscopy of Biological Systems; Clark, R. J. H., Hester, R. E., Eds.; Wiley: Chichester, UK, 1986; p 113–175.
30. Wang, Y.; Purrello, R.; Jordan, T.; Spiro, T. G. J Am Chem Soc 1991, 113, 6359–6368.
31. Matsoukas, J. M.; Hondrelis, J.; Keramida, M.; Mavromoustakos, T.; Makriyannis, A.; Yamdagni, R.; Wu, Q.; Moore, G. J. J Biol Chem 1994, 269, 5303–5312.
32. Carpenter, K. A.; Wilkes, B. C.; Schiller, P. W. Eur J Biochem 1998, 251, 448–453.